УДК 546.1

О воздействии тепловой и массовой дисперсии на синтез титаната бария методом CCSO

А.А. Марков

Институт проблем механики им. А.Ю. Ишлинского РАН
Россия, Москва, 119526, пр-т Вернадского, д. 101, корп. 1.
markov.ipm@yandex.ru

Аннотация

Излагаются результаты исследования воздействия тепловой и концентрационной дисперсии на синтез сложных оксидов при горении углерода (CCSO) в пористой среде. Представлен анализ литературы. Применен метод получения макроуравнений сохранения в пористой среде, основанный на усреднении по элементарному объему уравнений сохранения на микроуровне. Представлены решаемые макроскопические уравнения сохранения, включающие дисперсионный, конвективный и кондуктивный механизм тепло- и массопереноса в среде, состоящей из реагирующих компонент газовой и твердой фаз. Произведено обезразмеривание решаемых уравнений. Представлено три кинетики синтеза. Результаты удовлетворительно согласуются с данными экспериментов. Сопоставлены расчеты, включающие воздействие дисперсии при заданной пористости с расчетами, пренебрегающими дисперсией. Представленные данные позволяют моделировать и оценить влияние дисперсии на CCSO, таких как фронт горения, скорость синтеза и однородность распределения в реакторе реагентов и продукта синтеза микронных частиц титаната бария.

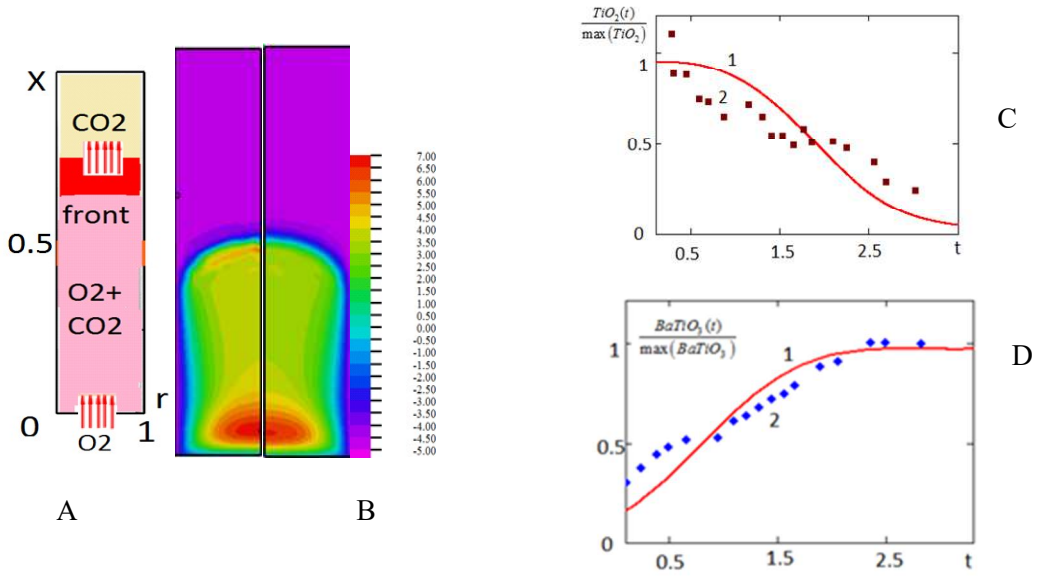

Схема реактора синтеза. Фронт движется снизу вверх. Кислород поступает снизу – (A). Температура твердой фазы (слева) и газовой фазы (справа) в момент времени $t = 0.1$ – (B). Плотность реагента, $TiO_2(t)$ отнесенная к $\max(TiO_2)$ – (C) и плотность продукта $BaTiO_3(t)$, отнесенная к $\max(BaTiO_3)$ – (D) как функция времени в точке образца с координатами $(2.5, 0)$ сравнивается с данными эксперимента [18], (символы)

On Thermal and Mass Dispersion Effect on Barium Titanate Synthesis via CCSO

A.A. Markov

Ishlinsky Institute for Problems in Mechanics RAS
Moscow, 119526, Russia
markov.ipm@yandex.ru

Abstract

This paper reports a study on thermal and mass dispersion in carbon combustion synthesis of oxides (CCSO) in a porous media. A well known volume averaging procedure of the microscopic conservation equations over an elementary volume is applied to derive the macroscopic conservation equations in a porous media. The approach allows us to account for the dispersion, convective and conductive heat and mass transfer in a porous media consisting of gas components mixture and solid particles of reactant species. The model developed in dimensionless variables using the similarity parameters is applied to numerical simulation of barium titanate micron particles synthesis using the thermal and mass dispersion effect. Three different kinetic schemes of synthesis are explored. The results are in satisfactory agreement with experimental measurements. The modeling with allowance for dispersion is compared to that one neglecting the dispersion. The data presented demonstrates the significant influence of the dispersion on CCSO process such as the combustion speed, the rate of synthesis and the uniformity of reagents and product distribution in the reactor.

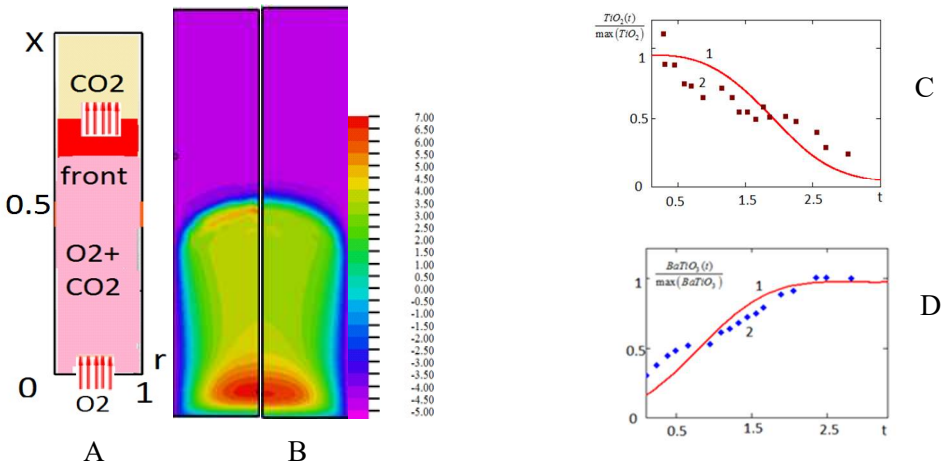

The schematic presentation of the combustion model. The front moves from bottom to top. Oxygen is supplied from the bottom (figure 1A). The temperature of solid phase (left) and gas (right) at time instance $t = 0.1$ is shown in figure 1B. The normalized reagent density $\mathrm{TiO_2}(t)$ referred to $\max(\mathrm{TiO_2})$ figure 1C and product density $\mathrm{BaTiO_3}(t)$ referred to $\max(\mathrm{BaTiO_3})$ figure 1D versus time at the sample location $(2.5, 0)$ on the axis of symmetry is compared with the experiment [18], (points)

1. Introduction

Thermal and mass dispersion may be characterized as a mechanism of transfer that occurs in moving gas or liquid in a porous media. While the molecular diffusion takes place in a flowing and stagnant media as well, the dispersion is strongly influenced by the hydrodynamic flow. Hydrodynamic/mechanical dispersion results from velocity variations, which arise from the velocity profile in a single pore, the velocity differences between different pores in the porous media and the tortuosity that occur in configurations of fluid moving across porous media systems. The fundamentals of the dispersion theory and further references can be found in [1–3]. The various methods and results of averaging in porous media are reviewed in [4]. The thermal and mass dispersion are effected by fluctuations of temperature and concentrations of species in multicomponent gas mixture in a porous media. The dispersion was applied in the literature [4–8]. The thermal dispersion was modelled as a tensor which components being either parallel or orthogonal to the main flow direction [5−7]. The dispersion thermal diffusivity was presented as the addition to the thermal (molecular) conductivity describing the longitudinal, transverse and lateral heat transfer. It was anticipated that the transverse and lateral dispersions are of the same order in core region of the porous media, but not in the region near the impermeable wall. The correlations for the longitudinal and transversal dispersion coefficients for mass transport are discussed in [5, 6]. Longitudinal dispersion values were consistently higher compared to their transversal counterparts. The transversal component of heat dispersion was modelled as a velocity dependent term, which is added to the thermal conductivity term in the energy equation. The dispersion concept explains the difference of transfer parameters measured along and across the main flow observed in the experiments [4]. Analysis carried on a Brinkman flow model [8], allows to conclude that dispersion affects to increase heat transfer while boundary and inertia effects to act contrarily.

The self-propagating high-temperature synthesis (SHS) was developed in numerous papers [9] where references can be found. A novel, modified SHS process using carbon combustion synthesis of oxides (CCSO) was suggested in [10]. The theory of complex oxides synthesis via combustion requires the multi-temperature models to be applied [11–18]. This formulation considers the reactor of synthesis by two coexisting temperature fields of the solid and fluid phases. In the presence of two temperature fields, there is an additional heat exchange between both phases, i.e., there is no local thermal equilibrium.

Because of its very high dielectric constant at room temperature, barium titanate ($BaTiO_3$) is one of the most important materials in ferroelectrics [18, 19]. Also, $BaTiO_3$ ceramics present a ferroelectric–paraelectric transition at the Curie temperature, showing the so-called positive temperature coefficient of resistivity (PTCR) effect. In the ceramic industry, $BaTiO_3$ powder is frequently obtained after calcinations of TiO_2 and $BaCO_3$ raw materials. Regarding this matter, industry requirements need to balance energy consumption, calcination time, and the quality of the final particulate product. Comprehension of the reaction kinetics allows to meet these industrial requisites [18, 19].

Physically, a porous medium is formed by a solid phase and one or more fluid phases. The solid may have a periodic or random structure, each phase may be continuous or dispersed and the characteristic sizes of the geometric heterogeneities may span a large range of length scales. These length scales can either differ by orders of magnitude (i.e. they are separated) or they may vary almost continuously in order of magnitude (i.e. they are continuous) [3, 4]. For particulate media, the geometric heterogeneities are the result of large differences in particle sizes and nonuniform distribution and agglomeration of particles with different sizes. For continuous media the heterogeneities are the result of size aspect ratio and spatial distribution of the solid phase. Chemically, the solid phase may be either inert or it may participate directly in the reactions as a catalytic surface or a source of fuel [5−8]. The complexity of interphase surfaces and structures of porous media requires the deriving the macroscopic conservation transfer equations by a volume averaging of the microscopic conservation equations over a representative volume [3–5].

The objective of present paper is to analyze the effects of hydrodynamic dispersion on the heat and mass transfer that occurs in CCSO. A volume averaging of the microscopic conservation equations over an elementary volume using [3] allows us to derive the macroscopic conservation equations for convective and conductive heat and mass transport in a porous mixture of gas components and solid powder of reactant species. The deviations of temperature and gas species densities from the corresponding mean values are applied as the dispersion terms caused by temperature and mass fluctuations [4−7]. The closure scheme of the set of governing equations is based on experimentally verified results [8] for gas-solid thermal nonequilibrium combustion. The model developed for dimensionless variables is numerically solved and applied to barium titanate synthesis using three kinetics [10, 18, 19]. The simulation results are in satisfactory agreement with experimental data [19]. The thermal dispersion strongly influences the thermal front propagation as well as the barium titanate synthesis rate.

2. Microscale balance equations

We begin with point-wise conservation equations in microscale volume V^{micro} for two phases gas and solid. Let gas and solid occupies the volume χV^{micro} and $(1-\chi)V^{micro}$ respectively, where χ is porosity. We suppose the continuum hypothesis and the thermodynamic equilibrium in micro volume and phase interfaces hold [20, 21]. We consider the energy conservation equations for gas and solid phases

$$\rho_g c_g \chi\left(\frac{\partial T_g}{\partial t}+\mathbf{u}\cdot\nabla T_g\right)=\nabla\cdot\left(\chi\lambda_g\nabla T_g\right)+\chi(1-\chi)Q_{reac} \tag{1}$$

$$\rho_S c_S (1-\chi)\frac{\partial T_S}{\partial t}=\nabla\cdot\left((1-\chi)\lambda_S\nabla T_S\right)+\chi(1-\chi)Q_{reac} \tag{2}$$

The conduction, advection and combustion heat are included. The gas and solid conductivities are taken in the form $\chi\lambda_g$ and $(1-\chi)\lambda_S$ [6,7], T_g, c_g is gas temperature and heat capacity of gas at constant pressure, λ_g is thermal conductivity of gas, T_S, c_S is temperature and heat capacity of solid, λ_S is solid thermal conductivity, Q_{reac} is the combustion heat that depends on kinetics and will be specified below.

Deriving the macro equations via the volume average approach

The volume-averaged balance of mass and energy is obtained from the averaging of the point-wise conservation equations (1), (2). Rigorous derivations of volume- averaged conservation equations are considered in [3−6]. The intrinsic phase- average of a scalar or vector quantity ψ_α is defined as the volume average of that quantity over the elementary representative region $\Omega(x_1,x_2,x_3)$ centred at point B with coordinates (x_1,x_2,x_3), where $\alpha=g$ for gas and $\alpha=\mathrm{s}$ for solid phase. The average value is defined as

$$\langle\psi_\alpha\rangle=\frac{1}{V}\int\limits_{\Omega_\alpha}\psi_\alpha \mathrm{d}V\,,\quad \alpha=g,\mathrm{s};\ \ \Omega=\Omega_g\cup\Omega_S$$

Let V be the volume of Ω and $V=V_g+V_S$, where V_g and V_S are the volumes of parts occupied by gas and solid respectively. The choice of the size of the elementary representative volume V is such that it is large compared to the pore- (or particle-) level geometric length scale d_p, but small compared to the averaging geometric length scale l_0. At the same time, l_0 must be much smaller than macro scale L (diameter of the reactor of synthesis), so the restriction $d_p \ll l_0 \ll L$ is supposed. The averaging of quantity ψ_α related to volume V_α is defined as

$$\langle \psi_\alpha \rangle^\alpha = \frac{1}{V_\alpha} \int\limits_{\Omega_\alpha} \psi_\alpha \mathrm{d}V,\ \alpha = g, \mathrm{s}$$

The formulas are valid $\langle \psi_g \rangle = \chi \langle \psi_g \rangle^g$, $\langle \psi_S \rangle = (1-\chi)\langle \psi_S \rangle^S$.

We apply below the averaging over a stagnant region supposing the solid phase is not moving and gas velocity is zero ($u = 0$) at the interphase surface. To derive the macroscopic equations from the microscopic equations, the following averaging theorems [3–5] relating the volume average of a spatial derivative to the spatial derivative of the volume average are needed:

$$\langle \nabla \cdot (\lambda_\alpha \nabla T_\alpha) \rangle = \nabla \cdot (\langle \lambda_\alpha \nabla T_\alpha \rangle) + \frac{1}{V} \int\limits_{A_{\alpha\beta}} \lambda_\alpha \nabla T_\alpha \cdot \mathbf{n}_\alpha \, \mathrm{d}A \tag{3}$$

$$\langle \lambda_\alpha \nabla T_\alpha \rangle = \lambda_\alpha \nabla (\langle T_\alpha \rangle) + \frac{1}{V} \int\limits_{A_{gS}} \lambda_\alpha T_\alpha \mathbf{n}_\alpha \, \mathrm{d}A,\ \alpha = g, \mathrm{s}, \tag{4}$$

where $A_{\alpha\beta}$ is the interface between the phases; $\mathbf{n}_\alpha$ is outer normal with respect to region Ω_α.

Using (1–4) and the volume averaging, we arrive at the energy conservation equations for gas and solid phases

$$C_{pg}\rho_g \chi \left(\frac{\partial}{\partial t} \langle T_g \rangle^g + \langle \mathbf{u} \rangle^g \cdot \nabla \langle T_g \rangle^g \right) = \nabla \cdot \left(\chi \lambda_g \nabla \left(\langle T_g \rangle^g \right) \right) + \langle Q_r \rangle +$$

$$+ \frac{1}{V_g} \int\limits_{A_{gS}} \left(\chi \lambda_g \nabla T_g \right) \cdot \mathbf{n}_g \, \mathrm{d}A + \nabla \cdot \left(\frac{1}{V_g} \int\limits_{A_{gS}} \chi \lambda_g T_g \, \mathbf{n}_g \, \mathrm{d}A \right),$$

$$C_S \rho_S (1-\chi) \frac{\partial}{\partial t} \langle T_S \rangle^S = \nabla \cdot \left((1-\chi) \lambda_S \langle \nabla T_S \rangle^S \right) + \langle Q_r \rangle +$$

$$+ \frac{1}{V_S} \int\limits_{A_{gS}} \left((1-\chi) \lambda_S \nabla T_S \right) \cdot \mathbf{n}_S \, \mathrm{d}A + \nabla \cdot \left(\frac{1}{V_S} \int\limits_{A_{gS}} (1-\chi) \lambda_S T_S \mathbf{n}_S \, \mathrm{d}A \right),$$

$\langle Q_r \rangle$ denotes the averaged combustion heat. Let the heat exchange terms using the interphase heat transfer coefficient κ be as follows [1, 2]:

$$\frac{1}{V_g} \int\limits_{A_{gS}} \left(\chi \lambda_g \nabla T_g \right) \cdot \mathbf{n}_g \, dA + \nabla \cdot \left(\frac{1}{V_g} \int\limits_{A_{gS}} \chi \lambda_g T_g \, \mathbf{n}_g \, dA \right) = \frac{A}{V} \kappa \left(\langle T_S \rangle^S - \langle T_g \rangle^g \right),$$

$$\frac{1}{V_S} \int\limits_{A_{gS}} \left((1-\chi) \lambda_S \nabla T_S \right) \cdot \mathbf{n}_S \, dA + \nabla \cdot \left(\frac{1}{V_S} \int\limits_{A_{gS}} (1-\chi) \lambda_S T_S \mathbf{n}_S \, dA \right) = -\frac{A}{V} \kappa \left(\langle T_S \rangle^S - \langle T_g \rangle^g \right),$$

A is the square of $A_{g,S}$.

Thermal and mass dispersion

Now we decompose the microscopic temperature into the sum of the intrinsic phase average (macroscopic) and a deviation of temperature marked by strike as $T_g = \langle T_g \rangle^g + T_g'$, $T_S = \langle T_S \rangle^S + T_S'$ The restrictions are implied [6, 8]

$$\langle \rho_g \rangle^g = \rho_g, \quad \langle \lambda_g \rangle^g = \lambda_g, \langle \lambda_S \rangle^S = \lambda_S, \quad \langle C_g \rho_g \rangle^g = C_g \rho_g, \quad \langle C_S \rho_S \rangle^S = C_S \rho_S \langle \mathbf{u} \rangle^g = \mathbf{u} \tag{5}$$

The velocity deviations are not considered. The averaged equation for gas temperature in the case of constant heat capacity at constant pressure C_{pg} reads

$$C_{pg}\rho_g\chi\left(\frac{\partial}{\partial t}\langle T_g\rangle^g+\langle\mathbf{u}\rangle^g\cdot\nabla\langle T_g\rangle^g\right)=\langle Q_r\rangle+\nabla\cdot\left(\left(\chi\lambda_g+\mathrm{D_{Tg}}\right)\nabla\langle T_g\rangle^g\right)-\frac{A}{V}\kappa\left(\langle T_g\rangle^g-\langle T_S\rangle^S\right)$$

The equation for solid phase at constant heat capacity using the averaging takes the form

$$C_S\rho_S(1-\chi)\frac{\partial}{\partial t}\langle T_S\rangle^S=\langle Q_r\rangle+\nabla\cdot\left((1-\chi)\lambda_S\nabla\left(\langle T_S\rangle^S\right)+\mathrm{D_{Ts}}\nabla\left(\langle T_S\rangle^S\right)\right)-\frac{A}{V}\kappa\left(\langle T_S\rangle^S-\langle T_g\rangle^g\right)$$

The closure modeling for thermal dispersion is given by tensors $\mathrm{D_{Tg}}$ and $\mathrm{D_{Ts}}$. The closure tensors can be written as follows:

$$\nabla\cdot\mathrm{D_{Tg}}\nabla\left(\langle T_g\rangle^g\right)=-C_{pg}\chi\rho_g\Psi_{Du}+\nabla\cdot\left(\chi\lambda_g\nabla T_g^{'}\right)+\frac{1}{V_g}\int\limits_{A_{gS}}\chi\lambda_g\nabla T_g^{'}\cdot\mathbf{n}_g\,\mathrm{d}A+\nabla\cdot\left(\frac{1}{V_g}\int\limits_{A_{gS}}\chi\lambda_g T_g^{'}\mathbf{n}_g\,\mathrm{d}A\right),$$

$$\Psi_{Du}=\left\langle\mathbf{u}\cdot\nabla T_g\right\rangle^g+\frac{1}{V_g}\left(\mathbf{u}\cdot\int\limits_{A_{gS}}T_g^{'}\mathbf{n}_g\,\mathrm{d}A\right)$$

$$\nabla\cdot\mathrm{D_{Ts}}\nabla\left(\langle T_S\rangle^S\right)=\nabla\cdot\left(\langle(1-\chi)\lambda_S\nabla T_S'\rangle^S\right)+\frac{1}{V_S}\int\limits_{A_{gS}}((1-\chi)\lambda_S\nabla T_S')\cdot\mathbf{n}_S\,\mathrm{d}A+\nabla\cdot\left(\frac{1}{V_S}\int\limits_{A_{gS}}(1-\chi)\lambda_S T_S'\mathbf{n}_S\,\mathrm{d}A\right)$$

The similar procedure of averaging mass conservation equation for oxygen and carbon dioxide results in the equations

$$\frac{\partial}{\partial t}\left(\langle\chi\rho_{jg}\rangle^g\right)+\nabla\cdot\left(\langle\mathbf{u}\rangle^g\langle\chi\rho_{jg}\rangle^g\right)=\langle J_{jm}\rangle^g+\nabla\cdot\left(\langle D\chi\rho_g\rangle^g\nabla\left(\langle C_j\rangle^g\right)+\chi\rho_g\mathrm{D_{mg}}\nabla\left(\langle C_j\rangle^g\right)\right),\ j=1,2,$$

$$\nabla\cdot\left(\chi\rho_g\mathrm{D_{mg}}\nabla\left(\langle C_j\rangle^g\right)\right)=-\chi\rho_g\Psi_{Cu}+\nabla\cdot\left(D\chi\rho_g\nabla\left(\langle C_j'\rangle^g\right)\right)+\nabla\cdot\left(D\chi\rho_g\frac{1}{V_g}\int\limits_{A_{gS}}C_j'\mathbf{n}_g\,\mathrm{d}A\right),$$

$$\Psi_{Cu}=\langle\mathbf{u}\rangle^g\cdot\nabla\langle C_j\rangle^g+\frac{1}{V_g}\langle\mathbf{u}\rangle^g\cdot\int\limits_{A_{gS}}C_g'\,\mathrm{d}A$$

Here the terms Ψ_{Tu} and Ψ_{Cu} present the gas velocity impact into mass dispersion, $\langle J_{jm}\rangle^g$ is mass flux due to chemical conversion of density ρ_{jg} in combustion, $\rho_{1g}=\rho_{\mathrm{O_2}}$, $\rho_{2g}=\rho_{\mathrm{CO_2}}$, $C_1=\rho_{\mathrm{O_2}}\rho_g^{-1}, C_2=\rho_{\mathrm{CO_2}}\rho_g^{-1}$.

We apply the closure model [8], developed to study the heterogeneous combustion and satisfactory agreed with experimental measurements.

$$\lambda_{g\Sigma}=\lambda_g+\lambda_D,\quad \mathrm{D_{Tg}}=(\lambda_D)\mathrm{I},\quad \lambda_D=\lambda_g\left(b_0Pe_t+b_1Pe_t\ln(Pe_t)\right),$$

$$D_{g\Sigma}=D+D_m^1\chi,\quad \mathrm{D_{mg}}=\left(D_{md}^1\chi\right)\mathrm{I},\ D_{md}^1=D\left(b_0Pe_m+b_1Pe_m\ln Pe_m\right),$$

were I is the unit tensor; $|\mathbf{u}|$ is the norm of velocity vector; d_p is the particle diameter; D is the diffusivity; a_g is the gas thermal diffusivity; $\lambda_{S\Sigma}=\lambda_S$, i.e. the thermal dispersion of solid phase is not considered, The local Peclet numbers read [8]

$$\mathrm{Pe}_t = \frac{\chi |\mathbf{u}| d_p}{2a_g}, \quad \mathrm{Pe}_m = \frac{\chi |\mathbf{u}| d_p}{2D}$$

Three kinetics of $BaTiO_3$ synthesis

We consider the three models of kinetics for barium titanate synthesis [10, 18].

I. $BaCO_3$ precursor

$$\mathrm{O_2 + C \xrightarrow[Q_1]{k_1} CO_2},\ \mathrm{BaCO_3 \xrightarrow[Q_2]{k_2} CO_2 + BaO},\ \mathrm{TiO_2 + BaO \xrightarrow[Q_2]{k_2} BaTiO_3},$$
$$\mathrm{BaO + BaTiO_3 \xrightarrow[Q_3]{k_3} Ba_2TiO_4},\ \mathrm{TiO_2 + Ba_2TiO_4 \xrightarrow[Q_3]{k_3} 2BaTiO_3}$$

II. BaO precursor

$$\mathrm{O_2 + C \xrightarrow[Q_1]{k_1} CO_2},\ \mathrm{TiO_2 + BaO \xrightarrow[Q_2]{k_2} BaTiO_3},\ \mathrm{BaO + BaTiO_3 \xrightarrow[Q_3]{k_3} Ba_2TiO_4}$$
$$\mathrm{TiO_2 + Ba_2TiO_4 \xrightarrow[Q_3]{k_3} 2BaTiO_3}$$

III. BaO_2 precursor

$$\mathrm{O_2 + C \xrightarrow[Q_1]{k_1} CO_2},\ \mathrm{TiO_2 + BaO \xrightarrow[Q_2]{k_2} BaTiO_3},\ \mathrm{2BaO_2 + TiO_2 \xrightarrow[Q_2]{k_2} Ba_2TiO_4 + O_2},$$
$$\mathrm{Ba_2TiO_4 \xrightarrow[Q_3]{k_3} BaTiO_3 + BaO}$$

For the $BaCO_3$ precursor kinetics the combustion heat is written as follows:

$$\langle Q_r \rangle = k_1 \chi Q_1 (1-\chi) \left\langle \rho_{\mathrm{O_2}} \right\rangle^g \langle \rho_{\mathrm{C}} \rangle^S \exp\left(-\frac{E_1}{R \left\langle T_g \right\rangle^g} \right) + k_2 Q_2 (1-\chi) \left\langle \rho_{\mathrm{BaCO_3}} \right\rangle^S \exp\left(-\frac{E_2}{R \left\langle T_g \right\rangle^g} \right)$$

Macro dimensionless governing equations

We apply the reference time scale t_0, $t_0 = 10(s)$, related to activation energy E and preexponential factor in the reaction rate expression k_1, [17]. The height and radius of the porous sample are $l_0 = 0.0007(\mathrm{m}), r_0 = 0.07(m)$, the gas velocity u_0 related to combustion speed in CCSO is $u_0 = 7 \times 10^{-4}\,(\mathrm{m/s})$ [16], $t_0 = k_1^{-1} \exp\left(E \times R^{-1} T_0^{-1}\right)$.

The dimensionless values marked by tilde for dimensional ones are presented below (the averaging symbol is omitted).

$$\tilde{x}_i = \frac{x_i}{l_0},\ \tilde{t} = \frac{t}{t_0},\ \tilde{u}_i = \frac{u_i}{u_0},\ \tilde{p} = \frac{p}{p_0},\ u_0 = \frac{l_0}{t_0}, \quad i = 1,2,3,$$

$$\rho_g = \rho_{1g} + \rho_{2g}, \tilde{\rho}_g = \frac{\rho_g}{\rho_0},\ \tilde{\rho}_{jg} = \frac{\rho_{jg}}{\rho_0},\ j = 1,2,\ \tilde{\rho}_S = \frac{\rho_S}{\rho_0}; \tilde{c}_{pg} = \frac{C_{pg}}{c_p},\ \tilde{D} = \frac{D}{D_0},$$

$$M_0 = m_{\mathrm{O_2}} + m_{\mathrm{CO_2}},\ \tilde{\lambda}_g = \frac{\lambda_{air}}{\lambda_0},\ \tilde{\lambda}_S = \frac{\lambda_S}{\lambda_0},\ \tilde{c}_S = \frac{C_S}{c_p},\ Ma^{-2} = \frac{\gamma_{air} p_0}{\rho_0 u_0^2},\ \mathrm{Re} = \frac{l_0^2}{t_0 \nu_{air}},$$

$$\mathrm{Pe}_T = \frac{l_0^2 \rho_0 c_p}{t_0 \lambda_0},\ \mathrm{Pe}_1 = \frac{l_0^2}{t_0 D_0},\ \tilde{Q} = \frac{Q t_0 k_1}{\rho_0 C_{pg} T_0},\ \tilde{k}_j = \frac{t_0 k_j}{\rho_0},\ j = 1,2,3,\ p_0 = \frac{R \rho_0 T_0}{M_0} \qquad (6)$$

Here $A=\pi r_0^2$; $V=l_0\times A$; $\rho_0=\rho_{air}=0.4\,(\mathrm{kg\cdot m^{-3}})$; $\lambda_0=\lambda_{air}=0.06\,(\mathrm{W/m/K})$; $D_0=2\times10^{-5}\,(\mathrm{m^2/s})$; $c_p=C_{p,air}=1114\,(\mathrm{J/(kg\cdot K)})$; $\nu_{air}=9.7\times10^{-5}\,(\mathrm{m^2/s})$; $\rho_S=\rho_{C(S)}$; $\rho_{1g}=\rho_{O_2(g)}$; $\rho_{2g}=\rho_{CO_2(g)}$ are species density; T_g,T_S are the temperatures of gas and solid phases that can be found using formulas $T_g=T_0\left(1+\beta\tilde{T}_g\right)$, $T_S=T_0\left(1+\beta\tilde{T}_S\right)$; $\tilde{\kappa}_0=\kappa_0 t_0 A/\left(c_p\rho_0 V\right)$ is the dimensionless heat transfer coefficient; $\tilde{c}_S,\tilde{c}_{pg}$ are the heat capacities; $\tilde{\lambda}_S,\tilde{\lambda}_g$ are the heat conductivities; $\tilde{D}$ is the mass diffusivity; Ma, Re are the Mach and Reynolds numbers; $\mathrm{Pe}_T,\mathrm{Pe}_1$ are the thermal and diffusion Peclet numbers, subscript *air* is referred to the air parameters at normal condition. The main dimensionless parameters related to activation energy and combustion heat are $\beta=RT_0/E$, $\gamma=c_P T_0\beta/Q$ [17]. R,E,Q are the gas constant, activation energy and combustion heat. In our numerical simulation the following values are applied $\beta\approx0.1$, $\gamma\approx0.2$. ($T_0\approx900K$), $k_1=10$, $k_2=0.5$, $k_3=0.1$, $Q_1=60$, $Q_2=0.1$.

For the sake of brevity, we use the numbered subscripts for molar masses and mass densities of species according the notations

$$M_{1g}=m(\mathrm{O_2}),\ M_{2g}=m(\mathrm{CO_2}),\ M_{1S}=m(\mathrm{C}),\ M_{2S}=m(\mathrm{BaCO_3}),\ M_{3S}=m(\mathrm{BaO}),$$

$$M_{5S}=m(\mathrm{BaTiO_3}),\ M_{6S}=m(\mathrm{Ba_2TiO_4}),$$

$$\rho_{1g}=\rho_{\mathrm{O_2}},\ \rho_{2g}=\rho_{\mathrm{CO_2}},\ \rho_{1S}=\rho_{\mathrm{C}},\ \rho_{2S}=\rho_{\mathrm{BaCO_3}},\ \rho_{3S}=\rho_{\mathrm{BaO}},$$

$$\rho_{4S}=\rho_{\mathrm{TiO_2}},\ \rho_{5S}=\rho_{\mathrm{BaTiO_3}},\ \rho_{6S}=\rho_{\mathrm{Ba_2TiO_4}}$$

We write down the governing equations (tilde is omitted) for variables (6) and kinetic scheme (I) [16, 17] using the molar masses and heat capacities relations as follows.

$$\frac{M_{1g}}{M_S}+1=\frac{M_{2g}}{M_S},\quad \frac{M_{1g}}{M_S}c_{1g}+c_{1S}=\frac{M_{2g}}{M_S}c_{2g},$$

$$c_{2S}=c_{2g}\frac{M_{2g}}{M_{2S}}+c_{3S}\frac{M_{3S}}{M_{2S}},\ c_{4S}=c_{5S}\frac{M_{5S}}{M_{4S}}-c_{3S}\frac{M_{3S}}{M_{4S}},\ c_{6S}\frac{M_{6S}}{M_{4S}}=c_{3S}\frac{M_{3S}}{M_{4S}}+c_{5S}\frac{M_{5S}}{M_{4S}},$$

were M_{ig},M_{jS} are molar masses; c_{ig}, c_{jS} are heat capacities, $i=1,2$, $j=1,...,6$.

The total mass conservation for gas and solid read

$$\frac{\partial\chi\rho_g}{\partial t}+\nabla\cdot\left(\chi\rho_g\,\mathbf{u}\right)=J_{S\to g},\ \frac{\partial(1-\chi)\rho_S}{\partial t}=-J_{S\to g},\quad J_{S\to g}=\chi(1-\chi)\rho_S\rho_{1g}k_1\exp\left(\frac{T_g}{\beta T_g+1}\right) \tag{7}$$

The mass conservation for gas species O_2, CO_2 are

$$\frac{\partial\chi\rho_g C_1}{\partial t}+\nabla\cdot\left(\chi\rho_g C_1\mathbf{u}\right)=\nabla\cdot\left(\frac{D_{g\Sigma}}{Pe_1}\rho_g\nabla C_1\right)-\frac{M_{1g}}{M_S}J_{S\to g},\ C_2=1-C_1,$$

$$\rho_{\mathrm{O_2}}=\rho_g C_1,\ \rho_{\mathrm{CO_2}}=\rho_g C_2 \tag{8}$$

$$D_{g\Sigma}=\chi\left(1+b_0Pe_m+b_1Pe_m\ln Pe_m\right)$$

In reactions involving solid species, reactants are not mixed on an atomic level, and they must diffuse into each other to propagate the reaction within the solid phase. Then, in the TiO_2+BaO system, subsequent $BaTiO_3$ formation is controlled by diffusion of barium ions through the $BaTiO_3$ layer [19]. The mass conservation equations for solid species according the kinetics (I) and including

the diffusion of BaO which depends on specie $BaTiO_3$ concentration [19] may be presented in the form

$$\frac{\partial \rho_{1S}}{\partial t} = -J_{1S}, \quad \frac{\partial \rho_{2S}}{\partial t} = -J_{2S}, \quad \frac{\partial \rho_{3S}}{\partial t} = \frac{M_{3S}}{M_{2S}} J_{2S} - \frac{M_{3S}}{M_{4S}} \left(J_{3S} + J_{4S} \right) J_{3S} + Ds_0 \exp\left(-\beta_D \rho_{5S}\right),$$

$$\frac{\partial \rho_{4S}}{\partial t} = -J_{3S} - J_{5S}, \quad \frac{\partial \rho_{5S}}{\partial t} = \frac{M_{5S}}{M_{4S}} \left(J_{3S} - J_{4S} + 2J_{5S} \right), \quad \frac{\partial \rho_{6S}}{\partial t} = \frac{M_{5S}}{M_{4S}} \left(J_{4S} - J_{5S} \right), \qquad (9)$$

were Ds_0 is a coefficient involving the diffusion of the migrating specie BaO, $\beta_D = 0.092$, $Ds_0 = 0.1$.

The fluxes for reactions (I) are:

$$J_{1S} = \chi (1-\chi) \rho_{1S} \rho_{1g} k_1 \exp\left(\frac{T_g}{\beta T_g + 1} \right), \; J_{2S} = (1-\chi) \rho_{2S} k_2 \exp\left(\frac{T_g}{\beta T_g + 1} \right),$$

$$J_{3S} = (1-\chi)^2 \rho_{3S} \rho_{4S} k_2 \exp\left(\frac{T_g}{\beta T_g + 1} \right), \; J_{4S} = (1-\chi)^2 \rho_{5S} \rho_{4S} k_3 \exp\left(\frac{T_g}{\beta T_g + 1} \right),$$

$$J_{5S} = (1-\chi)^2 \rho_{6S} \rho_{4S} k_3 \exp\left(\frac{T_g}{\beta T_g + 1} \right)$$

The momentum conservation equation of gas in porous media is applied in the form [4, 16].

$$\frac{\partial \chi \rho_g \mathbf{u}}{\partial t} + \nabla \cdot \left(\chi \rho_g \mathbf{u}\mathbf{u} \right) + \mathrm{Ma}^{-2} \nabla p = \mathrm{Re}^{-1} \nabla \cdot \boldsymbol{\tau} + S_V, \; \boldsymbol{\tau} = \mu \left[\nabla \mathbf{u} + (\nabla \mathbf{u})^T - \frac{2}{3} (\nabla \cdot \mathbf{u}) \mathbf{I} \right], \quad (10)$$

were $\mathbf{S_V}$ is resistance term [3,15], $(\mathbf{S_V})_j = -u_j \eta_j$, $\eta_j = \alpha_j |\mathrm{u}| + \varsigma_j$, $j = 1,2,3$; u_j are velocity components in Cartesian coordinate system; $p = \rho_g (1 + \beta T_g)$ is the gas pressure.

The heat balance equation for gas phase including the thermal dispersion reads

$$\rho_g c_{pg} \chi \left(\frac{\partial T_g}{\partial t} + \mathbf{u} \cdot \nabla T_g \right) + c_g T_g J_{S \to g} = \nabla \cdot \left(\chi \frac{\lambda_{g\Sigma}}{Pe_{Tg}} \nabla T_g \right) - \kappa \left(T_g - T_S \right) + Q_r, \qquad (11)$$

$$\lambda_{g\Sigma} = 1 + (b_0 Pe_t + b_1 Pe_t \ln Pe_t)$$

The heat balance equation for solid phase is written as

$$\rho_S c_S (1-\chi) \frac{\partial T_S}{\partial t} - c_S T_S J_{S \to g} = \nabla \cdot \left((1-\chi) \frac{\lambda_S}{Pe_{Ts}} \nabla T_S \right) + \kappa \left(T_g - T_S \right) + Q_r \qquad (12)$$

We apply the Leveqa's formula [20] describing the heat exchange between gas and solid phases

$$\kappa = \kappa_0 \left(1 + \mathrm{Re}_{loc}^{0.3} \, Pe_{Tloc}^{0.3} \right), \qquad (13)$$

were $\mathrm{Re}_{loc} = \mathrm{Re} |\mathbf{u}| \rho_g$, $\mathrm{Pe}_{Tloc} = \mathrm{Pe}_T |\mathbf{u}| \rho_g$ are local Reynolds and Peclet numbers [17].

The above system (7) – (12) of governing equations was applied with appropriate initial and boundary conditions on the lateral surface $r = 1$, axis of symmetry $r = 0$, inlet $x = 0$ and outlet $x = L$ of the reactor [17]. The thermal and oxygen fluxes were given on the inlet at the prescribed

time interval. The heat exchange with outer region was imposed on the lateral surface and outlet boundary.

Results of modelling and discussion

We present the simulation of barium titanate $BaTiO_3$ fine particles synthesis in the reactor region $0 < x < L,\ 0 < r < 1$ using the free heat exchange on lateral surface $r = 1, 0 < x < L$ and on the outlet $0 < r < 1, x = L$ for thermal exchange coefficient $\alpha_{ex} = 10^3$. The combustion is initiated by the thermal flux $q_f(t)$; $q_f(t) = Q_f, 0 \le t \le t_{init}$; $q_f(t) = 0, t \ge t_{init}$, and by the oxygen flux $O_{2f} = 100$ on the inlet (fig. 1A). At initial instance, the species densities of reagents were given and gas velocity was zero.

The results of CCSO modeling for the micron sized reagents and products were obtained for the following parameters [17]: $\alpha_j = 0,\ \varsigma_j = 50,\ t_{init} = 0.25,\ \chi = 0.5,\ \mathrm{Ma} = 0.01, Q_f = 500,\ Q = 60,$ $\mathrm{Re} = 0.1, \mathrm{Pe}_{Tg} = 0.2, \mathrm{Pe}_{Ts} = 0.4, \mathrm{Pe}_1 = 0.72$. The thermal and mass dispersion in barium titanate synthesis was simulated for $b_1 = 0$ see (12), porosity $\chi = 0.5$ and particle diameter $d_p = 3\times10^{-4}(\mathrm{m})$.

The reactor region is shown schematically in fig. 1A. The combustion wave propagates from bottom to top through the porous medium consisted of gas and solid particles. The product of synthesis is produced behind the combustion front. During the front movement, the CO_2 flow is generated and the O_2 and CO_2 mixture flow propagates upward. The combustion was initiated by a heat flux supplied from the bottom. The difference between the temperature of solid and gas phases in fig. 1B is not remarkable except the region close to combustion front. The result of barium titanate synthesis in fig. 1C, 1D is satisfactory agreement with experimental data [19].

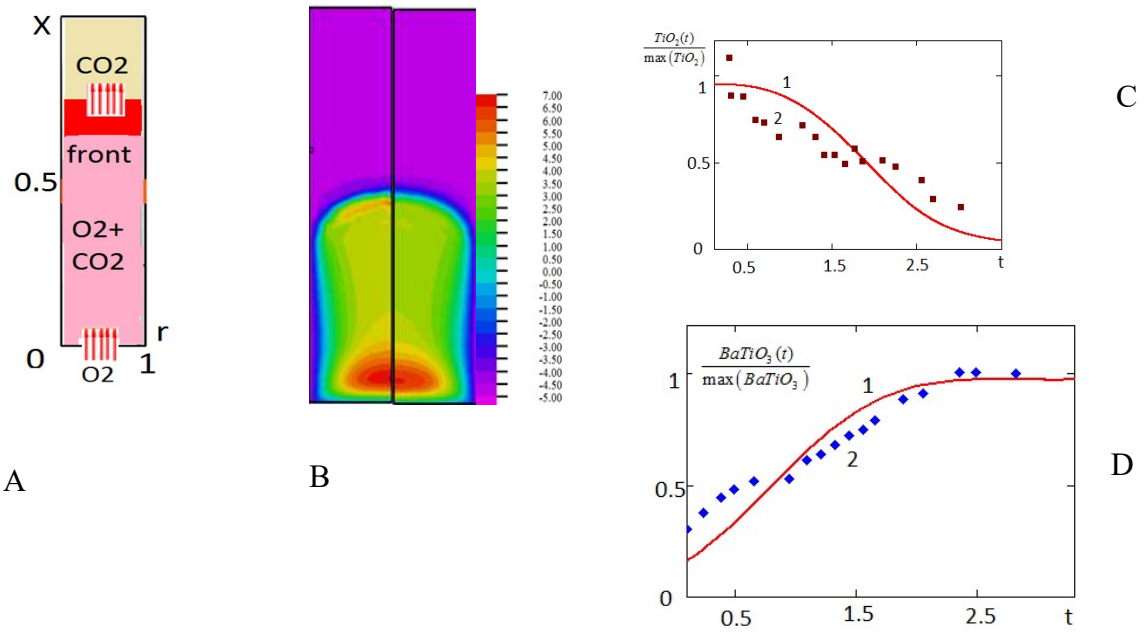

Fig. 1. The schematic presentation of the combustion model. The front moves from bottom to top. Oxygen is supplied from the bottom (fig. 1A). The temperature of solid phase (left) and gas (right) at time instance $t = 0.1$ is shown in fig. 1B. The normalized reagent density $TiO_2(t)$ referred to $\max(TiO_2)$ fig. 1C and product density $BaTiO_3(t)$ referred to $\max(BaTiO_3)$ fig. 1D versus time at the sample location $(2.5, 0)$ on the axis of symmetry is compared with the experiment [18], (points)

The density distribution of reagent TiO_2 (figs. 2A and 2B) and the product $BaTiO_3$ (figs. 2C and 2D) presented at the time instance $t = 0.5$ (figs. 2A and 2C) and $t = 2.5$ (figs. 2B and 2D) illustrates the solid species formation in the reactor region using the kinetics (I) ($BaCO_3$ precursor)

for $\chi = 0.5$, $\alpha_{ex} = 10^3$ and heat transfer $\kappa_0 = 1200$, see formula for heat transfer (13). Note the fastest rate of barium titanate synthesis for kinetics (III), about 90 % of reactor is occupied by $BaTiO_3$ at time instance $t = 2.5$ (see fig. 2D).

The results in fig. 3 refer to $\chi = 0.5$, $\kappa_0 = 1200$, $\alpha_{ex} = 10^3$. The thermal and concentration dispersion intensifies the heat and mass transport. The temperature (solid curves) is higher compared to ones neglecting the dispersion (points). It is interesting to note the increasing thermal front propagating speed and lower rate of temperature decreasing behind the combustion wave caused by dispersion. This result is dshown via temperature maximum values and temperature against time variation illustrated in fig. 3.

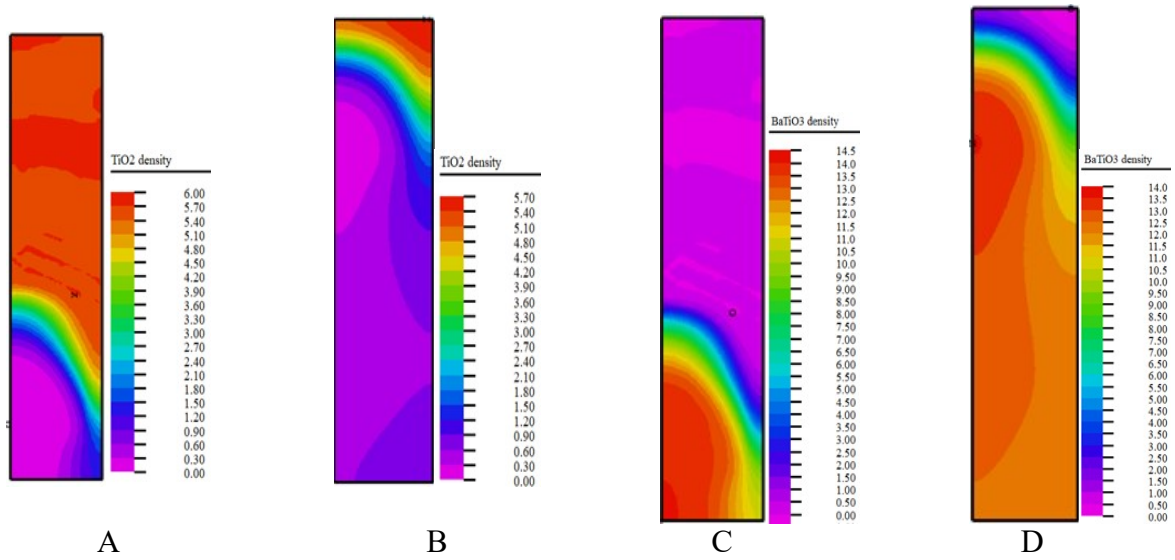

Fig. 2. The dynamics of reagent density TiO_2 (figures 2A and 2B) and the product density $BaTiO_3$ (figs. 2C and 2D) is presented at the time instance $t = 0.5$ (figs. 2A and 2C) and $t = 2.5$ (figs. 2B and 2D) using the kinetics (I) ($BaCO_3$ precursor) for $\chi = 0.5$, $\alpha_{ex} = 10^3$ and heat transfer $\kappa_0 = 1200$, see formula for heat transfer (13)

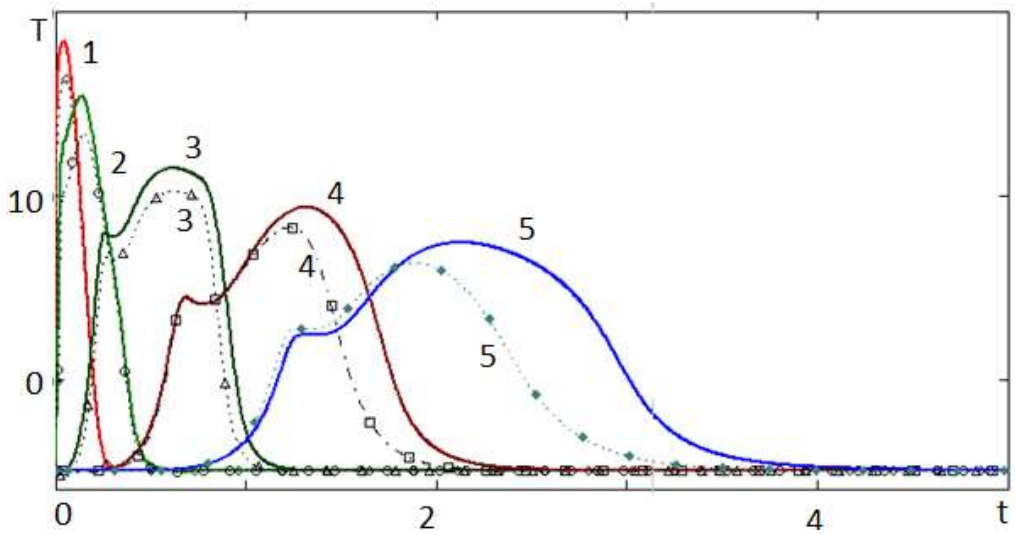

Fig. 3. Temporal axial temperature profile for locations (0,0), (0.25,0), (1.25,0), (2.5,0), (3.75,0) (curves and points 1,…,5 respectively) on the axis of symmetry is shown. The results of simulation with allowance for the dispersion effect (solid curves) is compared with no dispersion ones (points) using the precursor in barium titanate synthesis (kinetics (II))

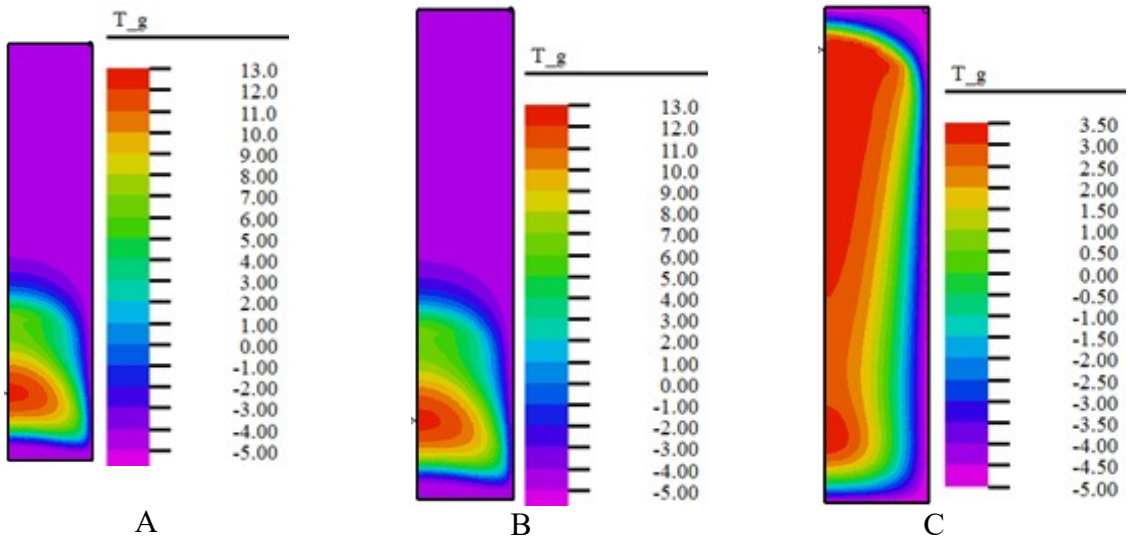

Fig. 4. The gas temperature distribution in the sample at time instance $t = 0.4$ is demonstrated for three kinetics (I), (II), (III) of barium titanate synthesis (figs. 4A, 4B, 4C respectively)

It is important to emphasize that oxygen release in kinetics (III) causes significant acceleration of thermal front propagating speed (fig. 4C as compared to figs. 4A and 4B). The values of temperature maximum in figs. 4A and 4B three times as higher than that one in fig. 4C. The transfer of some of the heat through the solid to the reactants in the gas phase results in the gas temperature increase and in turn, heat transfer to the solid.

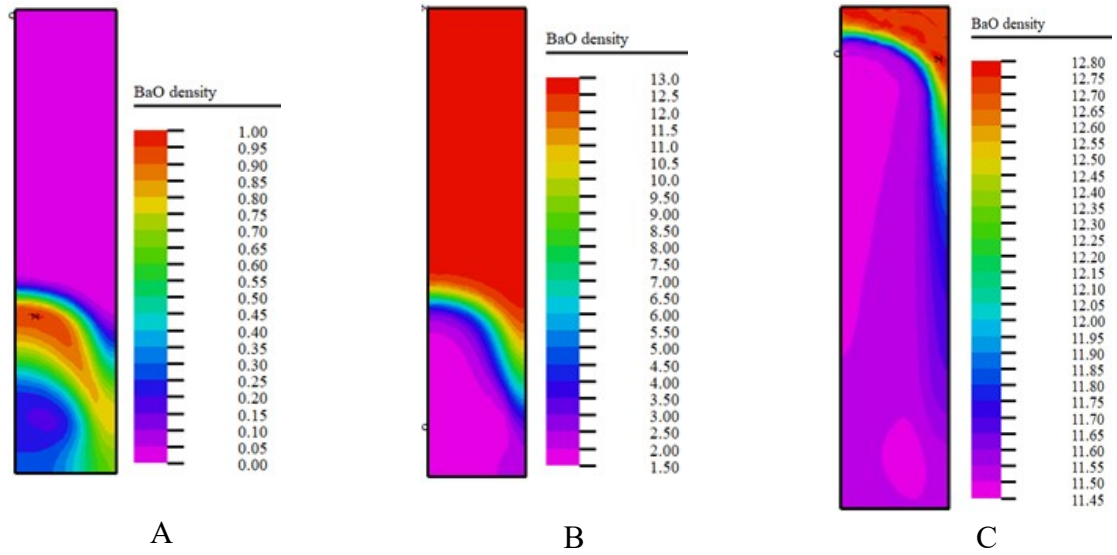

Fig. 5. The density of reagent BaO in the region of $BaTiO_3$ synthesis at time instant $t = 0.4$ is shown for three kinetics (I), (II), (III) – A, B, C respectively

According to kinetics (I) the initial value of reagent BaO is equal to zero while the prescribed nonzero initial value of BaO for kinetics (II) and (III) was given. According to the kinetics (I) the reagent BaO is produced in reaction of $BaCO_3$ decomposition and consumed in reactions of $BaTiO_3$ and Ba_2TiO_4 synthesis. These two conversion processes results in localized region of BaO nonzero density shown in fig. 5A. The acceleration of thermal front propagation for kinetics (III) causes the higher consumption of BaO region (fig. 5A) as compared to ones for kinetics (I) and (II) (figs. 5A and 5B).

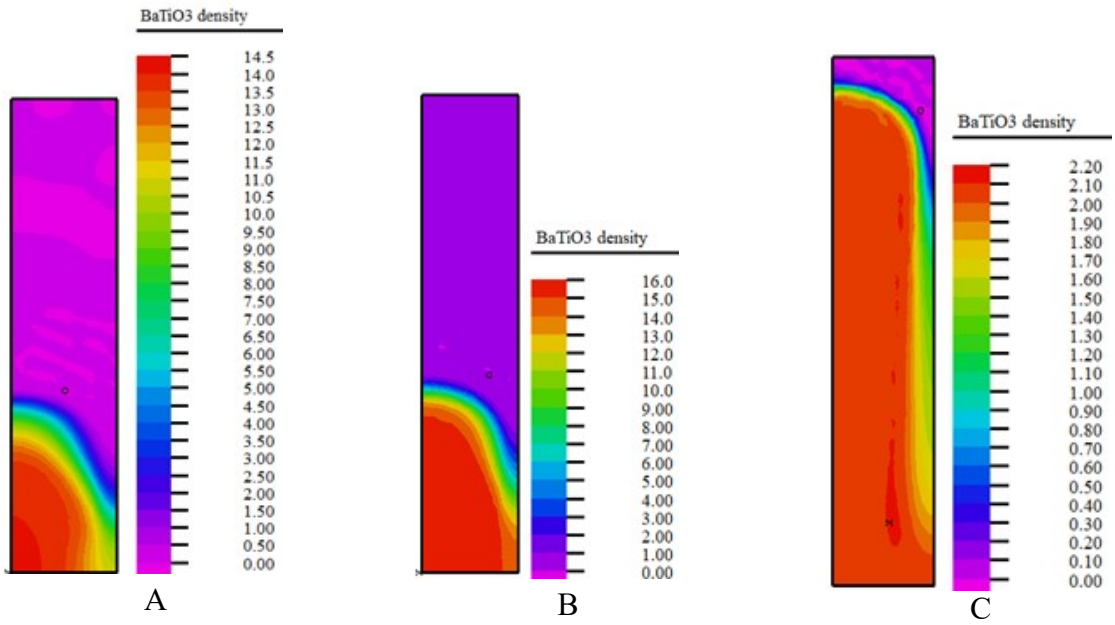

Fig. 6. The density of the product $BaTiO_3$ in the reactor region at time instance $t = 0.4$ is presented for kinetics (I), (II), (III) – A, B, C respectively

The results presented in figs. 2, 6 demonstrate the lower rate of barium titanate synthesis in region close to the lateral surface and outlet as compared to the core region of the reactor. This result is due to the cooling during heat exchange with outer media via transfer coefficient $\alpha_{ex} = 10^3$. The comparison results of modeling for (I), (II), (III) allow us to conclude the fastest synthesis rate for kinetics (III).

Conclusion

The generalization of CCSO model based on [17] with allowance for the thermal and mass dispersion (CCSOD) is presented and verified. The averaging procedure [3–5] using an elementary volume was applied to derive two temperature model equations including the deviations of temperature and of gas species concentration from the corresponding mean values. The closure of the set of governing equations is based on [8]. The analysis of thermal non-equilibrium between the gas and the solid phases was made by comparison computations with dispersion and that ones for the no-dispersion model. The intensification of transfer due to the dispersion was obtained in numerical simulation of CCSOD.

The application of CCSOD model was approved for barium titanate synthesis using three kinetics [10, 18, 19]. The simulation results are in satisfactory agreement with experimental data [18]. The thermal dispersion strongly influences the thermal front propagation rate. We may conclude that dispersion tends to increase heat transfer while boundary and inertia effects tends to act contrarily. The comparison of kinetics schemes for barium titanate synthesis showed the highest rate of synthesis for BaO_2 precursor kinetics scheme. The distribution of reagents and products in the reactor region allows us to analyze the dependence of uniformity of species caused by the thermal heat exchange between phases and outer region.

Acknowledgement

The present work was supported by the Ministry of Science and Higher Education within the framework of the Russian State Assignment under contract No. AAAA-A17-117021310376–4.

References

1. Whitaker S. Transport equations for multi-phase systems Chemical Engineering Science. 1973, vol. 28, pp 139−147.
2. Quintard M. and Whitaker S. Theoretical Analysis of Transport in Porous Media (ed Marcel Dekker, New York). 2000.
3. Amhalhel G.A. and Furmański P. Problems of modeling flow and heat transfer in porous media Biuletyn Inst Tech Cieplnej Politechniki Warszawskiej. 1997, No 85, pp 56−87.
4. Hsu C.T. and Cheng P. Thermal dispersion in a porous medium Int. J. Heat Mass Transf. 1990, 33. pp 1587–97.
5. Oliveiral A.A.M. and Kaviany M. Nonequilibrium in the transport of heat and reactants in combustion in porous media. Progress in Energy and Combustion Science. 2001, 27, pp 523−45.
6. Rubens S.T. and Osvair V. Dispersion in heat and mass transfer natural convection along vertical bounaries in porous media Faculdade de Engenharia Mecanica, Universidade Estadual de Campinas, 1308 I Campinas-SP Brazil. 1992.
7. Chen K., Martirosyan K.S. and Luss D. Hot Zones Formation during Regeneration of Diesel Particulate Filters AIChE J. February **57** 2 2011, pp 497−506.
8. Fatehi M. and Kaviany M. Role of gas-phase reaction and gas-solid thermal nonequilibrium in reverse combustion Int. Heat Mass Transfer. 1997, 11, pp 2607−2620.
9. Merzhanov A.G. Self-propagating high-temperature synthesis: Twenty years of research and findings In: Combustion and Plasma Synthesis of High-Temperature Materials eds Munir ZA, Holt JB. (New York, NY: VCH 1990.)
10. Martirosyan K.S. and Luss D. Carbon Combustion Synthesis of Oxides: Process Demonstration and Features AIChE J 51 2005, 10, pp. 2801−1280.
11. Dobrego K.V. and Zhdanok S.A. Engineering calculation of the characteristics of a filtration-combustion wave based on a one-dimensional two-temperature model J. of Engineering Physics and Thermophysics 1998, **71,** No 3.
12. Wahle C.W., Matkowsky B.J. and Aldushin A.P. Effects of Gas-Solid Nonequilibrium in Filtration Combustion Comb Sci and Tech. 2003, **175,** pp. 1389−1399.
13. Markov A.A., Filimonov I.A. and Martirosyan K.S. Two-Temperature Model and Simulation of Induced Electric Field During Combustion Synthesis of Zinc Sulfide in Argon Int. J. of Thermophysics 2019. **40** (1).
14. Markov A.A., Hobosyan M.A. and Martirosyan K.S. Investigation of ferrites synthesis behind a combustion wave using gas slip, temperature and gas species concentration jump on the pore surface of a solid phase//(in Russian). Physicochemical Kinetics in Gas Dynamics 2015 V16 (1). http://chemphys.edu.ru/issues/2015-16-1/articles/506/
15. Markov A.A., Hobosyan M.A. and Martirosyan K.S. Simulation of heat and mass transfer in pores as applied to synthesis of magnesium−zinc and nickel−zinc ferrite nanoparticles Nanomechanics Science and Technology: An Int. J. **6** (3)2015, pp 209-222 DOI: 101615/NanomechanicsSciTechnolIntJv6i340
16. Markov A.A., Filimonov I.A. and Martirosyan K.S. Modeling the Synthesis of Submicron-Sized Complex Oxides Theoretical Foundations of Chemical Eng. 2017, **51,** No 1, pp 27–37.
17. Brzozowski E., Sanchez J. and Castro1 M.S. BaCO3–TiO2 Solid State Reaction: A Kinetic Study J. of Materials Synthesis and Processing. 2002, **10**, No 1.
18. Beauger A., Mutin J.C. and Niepce J.C. Synthesis reaction of metatitanate BaTi03 Part 1 Effect of the gaseous atmosphere upon the thermal evolution of the system BaCO3-Ti02 J. of Materials Science 1983, 18, pp 3041−3046.
19. Frank-Kamenetskii D.A. Diffusion and Heat Transfer in Chemical Kinetics (Moscow: Nauka Press) 1987, p. 491.
20. Bird R B, Sewart W E and Iightfoot F N I960 Transport phenomena (New York: Wiley) p. 750.

Статья поступила в редакцию 20 марта 2020 г.